

Polymeric peptide pigments with sequence-encoded properties

Ayala Lampel¹, Scott McPhee¹, Hang-Ah Park², Gary G. Scott³, Sunita Humagain^{4,5}, Doeke R. Hekstra⁶, Barney Yoo⁷, Pim W.J.M. Frederix⁸, Tai-De Li¹, Rinat R. Abzalimov¹, Steven G. Greenbaum^{4,5}, Tell Tuttle³, Chunhua Hu,⁹ Christopher J. Bettinger^{2,10,11}, Rein V. Ulijn^{1,5,7*}

¹Advanced Science Research Center (ASRC), City University of New York, 85 St Nicholas Terrace, New York, NY 10031, USA.

²Department of Materials Science and Engineering, Carnegie Mellon University, 5000 Forbes Avenue, Pittsburgh, PA, 15213, USA.

³WestCHEM/Department of Pure & Applied Chemistry, University of Strathclyde, 295 Cathedral Street, Glasgow G1 1XL, UK.

⁴Department of Physics and Astronomy, Hunter College, City University of New York, 695 Park Avenue, New York, NY 10065, USA.

⁵The Graduate Center of the City University of New York, New York 10016, USA.

⁶Department of Molecular and Cellular Biology; School of Engineering and Applied Sciences; FAS Center for Systems Biology, Harvard University, Cambridge, MA 02138, USA.

⁷Department of Chemistry, Hunter College, City University of New York, 695 Park Avenue, New York, NY 10065, USA.

⁸Groningen Biomolecular Sciences and Biotechnology Institute, Rijksuniversiteit Groningen, The Netherlands.

⁹ Department of Chemistry, Silver Center for Arts and Science, 100 Washington Square East, New York University, New York, NY 10003, USA.

¹⁰Department of Biomedical Engineering, Carnegie Mellon University, 5000 Forbes Avenue, Pittsburgh, PA, 15213, USA.

¹¹McGowan Institute of Regenerative Medicine, 450 Technology Drive, Suite 300, Pittsburgh, PA, 15219, USA.

*Corresponding author. E-mail: rein.ulijn@asrc.cuny.edu

Melanins are a family of heterogeneous polymeric pigments that provide UV protection, structural support, coloration and free radical scavenging. Formed by oxidative oligomerization of catecholic small molecules, the physical properties of these materials are influenced by covalent and non-covalent disorder. We report the use of tyrosine-containing tripeptides as tunable precursors for polymeric pigments. In these structures, phenols are presented in a (supra-)molecular context dictated by the

peptide sequence by repositioning amino acids. Oxidative polymerization can be tuned in a sequence dependent manner resulting in peptide sequence-encoded properties such as UV absorbance, morphology, coloration and electrochemical properties over a considerable range. Short peptides have low barriers to application and can be easily scaled, suggesting near-term applications in cosmetics and biomedicine.

Controlled disorder in polymeric pigments by sequence-specific assembly of tripeptide precursors.

Melanin pigments are found in most life forms, from plants to bacteria to fungi and animals, where they have cardinal roles in organisms' coloration and protection from various (mainly photo- or free radical induced) cell damage-causing stresses (1). In addition to their protective roles, melanin pigments exhibit dynamic coloration and optoelectronic properties, inspiring efforts to design energy storage devices (2), environmental sensors (3) surface-adherent coatings (4-5) and colored films (6). The self-assembly and polymerization of natural melanin is regulated through complex pathways that include catalysis, templating, assembly, oxidation under confinement, in a process that is currently not fully understood (1). Laboratory-based strategies to synthesize melanin-based analogues are challenging to employ and difficult to control. Heterogeneous products typically consist of insoluble polymers with poorly defined chemical and structural composition (7), thereby limiting the technological utility of this class of materials.

We reasoned that supramolecular materials (8-9) formed by peptide building blocks (10-12) may offer promise for the formation of synthetic melanin-like materials (or polymeric pigments) due to the ability to precisely control the presentation of chemical functionality and consequently reactivity, through non-covalent interactions. Even very short peptides, consisting of only two or three amino acids (13-16) have been shown to self-assemble to form discrete nanoscale materials (17). Furthermore, combining supramolecular self-assembly with catalytic [enzymatic (18-19); or chemical (20-21)] transformations provides spatiotemporal control (22) over the assembly process, giving rise to materials with kinetically tunable properties. Thus, combining catalysis and self-assembly offers an attractive approach for aqueous materials processing (22-23).

Our first objective was to identify a small subset of peptides that self-assemble into supramolecular nanostructures with sequence-dependent properties. We focused on tyrosine (Y) containing tripeptides combined with the aggregation-prone aromatic amino acid phenylalanine (F) (14-15) and a charged amino acid, aspartic acid (D) (Fig. 1A). To increase self-assembly propensity at neutral pH conditions, C-terminal amides were used. All six possible tripeptide combinations were studied, with those that contain paired aromatics expected to favor assembly (14, 15). Following annealing by temporary heating (to 75°C) and subsequent cooling to room temperature, the six peptides exhibit distinctive macroscopic appearances (Fig. 1B, upper panel). Those peptides with paired aromatics give rise to self-assembly, while FDY and YDF remain a clear solution. YFD forms an opaque gel, FYD forms a suspension composed of amorphous aggregates, DFY forms a translucent gel, while DYF forms macroscopically observed needle-like crystalline fibers, eventually giving rise to a self-supporting gel (Fig. S1; Movie S1; Movie S2).

We sought to leverage the variable peptide assemblies to control formation of polymeric pigments initiated by enzymatic oxidation of tyrosine residues. We used

tyrosinase from *Agaricus bisporus*, which typically oxidizes tyrosine into 3,4-dihydroxyphenylalanine (DOPA) and further oxidation products, including DOPA-quinone, DOPACHrome and dihydroxyindole eventually forming polymers from these reactive species (Fig. S2). Tyrosinase, which was previously shown to act upon self-assembled peptides (24) was added directly to the tripeptide assemblies (post annealing). A readily observable, variable color change emerged for all tripeptides following 4 h incubation with colors intensifying further over 24 h, resulting in light brown coloration of transparent solutions of FDY and YDF, beige coloration for the milky FYD suspension to brown-black colors for YFD, DYF and DFY, suggesting that the oxidized peptides polymerized to different extents (Fig. 1B, lower panel). As a control, we used tyrosine which rapidly oxidized and polymerized, as observed by the black color of the sample and the polymeric precipitate.

Nanoscale morphologies were determined by transmission electron microscopy (TEM) (Fig. 2A) and AFM showing that nanostructures' stiffness depends on peptide sequence (Fig. S3). YFD and DFY assemble into a dense network of nanofibrils, while needle-like crystalline fibers are seen in DYF (Fig. S4) with amorphous aggregates observed for the others. In order to assess supramolecular order, the crystallization of DYF provides a convenient starting point. Single crystal X-ray diffraction (XRD) (Table S1) revealed five main interfaces that stabilize the crystal lattice (Fig. 2B). Along the *x*-axis, the peptides form parallel β -sheets that extend laterally by two interfaces along the *y* direction: hydrogen bonding between the amide groups (1) and salt bridges of the aspartate carboxylate groups and terminal amines (2). Along the *z*-axis, the β -sheets are packed through hydrogen bonding of the tyrosine hydroxyl groups (3) and aromatic stacking (4) into a 3D lattice. Single crystals could also be obtained by slow cooling of YFD solution. XRD shows similar interactions to DYF but with different consequences: for YFD a single backbone-backbone hydrogen bond was observed between molecules (Fig. 2C, 2). The columns interact laterally by aromatic stacking (1), yielding two-dimensional planes of aromatically stacked groups, and by alternating hydrogen bonding networks coupling the aspartate/amine salt bridges (3), C-terminal amides and tyrosine hydroxyl groups through well-ordered water molecules (4). The consequence of the observed packing is a substantially different orientation of the paired aromatics (Fig. S5-S8)- in opposite (*anti*) or same (*syn*) orientations for DYF and YFD with respect to the peptide backbone.

To shed more light on the organization of the tripeptides, including those for which crystal structures could not be obtained under the assembly conditions, we used Fourier transform infrared spectroscopy (FTIR) (Fig. 2D). FDY, YDF and FYD did not show evidence of periodically organized intermolecular interactions, as indicated by broad bands at 1,652 cm^{-1} (internal amide) and 1,672 cm^{-1} (terminal amide) in the FTIR spectrum, which is in agreement with observed disorder by TEM. For the assembled DFY and DYF peptides, these bands redshift to 1,620-1,640 cm^{-1} and 1,658 cm^{-1} respectively, which suggests a β -sheet-like organization. The YFD spectrum implies a different packing geometry, with additional narrow, redshifted bands in the amide region, but an additional shift of the aspartate carboxylate band from 1,580 cm^{-1} to 1,560 cm^{-1} , implying intramolecular salt bridge formation with the amine group of the N-terminus in agreement with the crystal structure (Fig. 2C), which helps to stabilize paired aromatics in the *syn* configuration.

The six peptides show variable crystallinity (Fig. S9-S14). FYD, YFD, and DYF form highly crystalline materials and DFY shows lower crystallinity, evidenced by the peak

intensity and broadness. In contrast, FDY and YDF are amorphous materials. However, all the peptides share some common features in terms of molecular stacking, reflecting by the peaks at the ranges of 4.4-4.8 Å and 2.9-3.2 Å. In addition, the diffraction patterns of DFY and DYF are similar, indicating the structural resemblance of these two peptides.

In order to examine the relative stability of the different conformations of the monomers, MD simulations were carried out (25-26) (Fig. 2E-F). The results demonstrate that the six peptides have different preferential conformations which is reflected both in the assembled state and in solution, depending on a pair-wise manner on the positions of the aspartic acid. The following relationships exist: tyrosine and phenylalanine residues are presented in *anti* configuration, (**DXX**), or *syn* (**XXD**) which is in agreement with the crystal structures obtained. When the aspartic acid is in the central position (**XDX**) there is no well-defined structure with the dihedral between the aromatic ring.

We subsequently investigated whether the pair-wise sequence-dependent supramolecular order of the peptides influences enzymatic oxidation and further polymerization pathways. WAXS and solid phase FTIR data show loss of order with the strongest effect observed for **DXX**, less in **XXD**, while **XDX** remain disordered (Fig. 3A-C). The peptides showed loss of supramolecular order (Fig. 3A-B, Fig. S9-S14) while retaining few structural features corresponding to the molecular packing, according to the peaks at about 4.5 and 2.9 Å. The FTIR spectra (Fig. 3C) show narrow, redshifted absorptions of the amide group in FYD, YFD, DFY and DYF that disappear upon oxidation in favour of broad absorptions at 1,650-1,675 cm⁻¹. Additionally, tyrosine-specific ring modes are lost (*e.g.* 1,516 cm⁻¹) and a new band absorption assigned to quinone is observed around 1,680 cm⁻¹, confirming catechol oxidation.

HPLC analysis showed (near-)complete conversions of peptides to oxidation products for both the disordered (**XDX**) and highly ordered (**DXX**) peptides with lower conversions observed for disordered **XXD** (disordered FYD to a lesser extent compared to YFD (Table S2). Under the conditions examined, peptide assembly has a more pronounced effect on oxidation and polymerization compared to the position of the tyrosine within the tripeptides. Early stage conversions are higher for **XDX** peptides compared to the assembling counterparts (Fig. S15). However, early stage kinetics are similar for the non-assembling FDY and YDF. We conclude that the overall polymerization process is dictated by supramolecular order of the precursors and less by enzyme affinity.

LCMS data obtained after 24 h of oxidation reveal the expected catechol and quinone, as well as a wide range of dimeric and trimeric species with different connections (Fig. 3D-F, Table S3). It is clear from these data that there is again a pair-wise relationship, with **XDX** peptides giving rise to complete conversion of the precursors to oligomers and polymers, **XXD** giving medium conversion with intermediate polymerization and both **DXX** peptides giving rise to formation of extensive oligomeric and polymeric species (Table S3, Fig. 3D). In each case, the UV absorbance of polymeric species is significantly red-shifted from precursors, as would be expected for an extensive catechol/quinone network.

The polymers have distinct morphologies as seen by optical microscopy (Fig. 4A). While YFD_{ox} maintains a one-dimensional morphology, it forms much larger fibers,

suggesting a degree of lateral aggregation which may be facilitated by the positioning of 2D sheets of reactive aromatic species at interfaces, as seen in the crystal structure (Fig. 2C). DFY_{ox} polymerizes into extended 2D sheets while DYF_{ox} forms spheres. These morphologies, and the amorphous structures of the other oxidized peptides, were also observed by TEM (Fig. S16). While the DFY_{ox} sheets and YFD_{ox} fibers are found in the solid phase, the DYF_{ox} spheres remain dispersed in the aqueous buffer.

The most contrasting structures formed are evident in DXX_{ox} tripeptides showing high levels of polymerization accompanied with loss of order starting from similar molecular packing of the precursors. For these peptides, a subtle difference in sequence dictates the initial (crystalline fibers vs supramolecular fibers) and oxidized (spheres vs sheets) morphology. For DFY_{ox}, we propose that the *anti* conformation of aromatic side chains is favorable for polymerization along the length of the β -sheet, but also laterally between neighboring fibrils, eventually resulting in loss of supramolecular structures (fibrils) and formation of extended, micron-scale 2D sheets. Time course TEM analysis of DFY (Fig. S17) supports this mechanism for the fiber-to-sheet transition, revealing the formation of dark layers on the fibrils' surface (4 h); these layers further assemble and polymerize into 2D sheets that extend from the fiber surface (1 week). For DYF, a different orientation of tyrosine gives rise to an additional stabilizing interaction (Tyr-Tyr) within the DYF crystal lattice (27) (Fig. 2B). Oxidation of tyrosine eliminates H-bonding in these residues thereby disrupting the crystalline fiber and reconfiguring the peptides into spherical assemblies. These data are in agreement with the loss of the original packing and subsequent polymerization observed for both DFY_{ox} and DYF_{ox} by FTIR, WAXS and LCMS (Fig. 3).

The results show that supramolecular order in peptide precursors can be systematically converted into disordered polymeric pigments, resulting in variable characteristics that relate to their functionality (Fig. 4). UV-Vis measurements showed different broadband spectra with DFY showing absorption throughout the visible region (420-650 nm) and the high absorption observed for FYD possibly contributed by highly scattering aggregates (Fig. 4B). The observed maximum around 340 nm for YFD_{ox}, together with the LCMS (Fig. 3D-E) and HPLC analyses (Fig. S15D) suggest that the N-terminal positioning of the catechol results in a lower degree of connectivity and cross-linking.

Oxidized peptides were configured into cathodes in aqueous half-cell configurations. The charge storage capacity can provide an estimate of the concentration of redox-active components while the shape of the discharge curve can provide insight into the distribution of morphological phases. For this purpose, electrodes were fabricated by compacting peptide melanin powders into a stainless steel support mesh (Fig. 4C) (28). For all systems tested, the potentials become monotonically more negative during discharge, which confirms that these materials are largely disordered. DFY_{ox} 2D sheets exhibit the highest specific charge storage capacity, followed by DYF_{ox} (Fig. 4D-E) which is attributed to an increase in the concentration of redox active tyrosine-based derivatives (2, 29), and is confirmed by cyclic voltammetry CV (Fig. S18). Capacitive storage is the likely source of differential capacities in cathodes composed of YFD_{ox} versus FYD_{ox}, which are otherwise largely devoid of redox behavior as assessed by CV. The specific capacity of DFY_{ox} is comparable to that measured in natural eumelanin cathodes and less than that of the synthetic melanin-based cathodes. (Fig. S19). CV of DFY_{ox}-based cathodes showed multiple redox peaks that are not commonly observed in other types of natural and synthetic melanin-based pigments (30), attributed to presence of multiple types of polyphenols, with a variety of redox behavior. Electron

paramagnetic resonance (EPR) suggests that DFY_{ox} sheets exhibit the highest gravimetric concentration of radical content among the polymeric peptide pigments (Fig. S20, Table S4). We propose that relatively higher semiquinone concentrations correspond to not only higher overall concentrations of catechols, but also molecular configurations that permit comproportionation reactions. The attenuated EPR signal observed in the polymeric peptide pigments is consistent with this model owing to the smaller overall catechol concentrations and reduced catechol-catechol interactions compared to natural eumelanins.

We demonstrate the ability to leverage differential assembly and reactivity to achieve tunable polymeric pigments, and find that supramolecular order in precursors is inversely correlated to disorder in resulting polymers. This gives rise to control and tunability over the properties of the materials. We note that the possibility of marrying the diverse structures that can be accessed in short peptide assemblies with melanin-like properties facilitates fundamental studies related to how tunable functions are dictated by order as well as disorder. Moreover, short peptides have low barriers to application and can be easily scaled, suggesting short term applications in cosmetics and biomedicine.

References

1. P. Meredith, T. Sarna, (2006). *Pigment Cell Res.* **19**, 572-594 (2006).
2. Y. J. Kim, W. Wu, S. E. Chun, J. F. Whitacre, C. J. Bettinger, *Proc. Natl. Acad. Sci. USA* **110**, 20912-20917 (2013).
3. C. Shillingford, C. W. Russell, I. B. Burgess, J. Aizenberg, *ACS Appl. Mater. Interfaces* **8**, 4314-4317 (2016).
4. H. Lee, S. M. Dellatore, W. M. Miller, P. B. Messersmith, *Science* **318**, 426-430 (2007).
5. G. Fichman *et al.*, *ACS Nano* **8**, 7220-7228 (2014).
6. M. Xiao *et al.*, *ACS Nano* **9**, 5454-5460 (2015).
7. M. d'Ischia, A. Napolitano, V. Ball, C. T. Chen, M. J. Buehler, *Acc. Chem. Res.* **47**, 3541-3550 (2014).
8. M. J. Webber, E. A. Appel, E. W. Meijer, R. Langer, *Nat. Mater.* **15**, 13-26 (2016).
9. T. Aida, E. W. Meijer, S. I. Stupp, *Science* **335**, 813-817 (2012).
10. S. Zhang, *Nat. Biotechnol.* **21**, 1171-1178 (2003).
11. F. G. Omenetto, D. L. Kaplan, *Science* **329**, 528-531 (2010).
12. M. R. Ghadiri, J. R. Granja, R. A. Milligan, D. E. McRee, N. Khazanovich, *Nature* **366**, 324-327 (1993).
13. C. H. Görbitz, *Chem. Eur. J.* **7**, 5153-5159 (2001).
14. M. Reches, E. Gazit, *Science* **300**, 625-627 (2003).
15. P. W. J. M. Frederix *et al.*, *Nat. Chem.* **7**, 30-37 (2015).
16. S. Marchesan *et al.*, *Nanoscale* **4**, 6752-6760 (2012).
17. L. Adler-Abramovich, E. Gazit, *Chem. Soc. Rev.* **43**, 6881-6893 (2014).
18. B. H. Hu, P. B. Messersmith, *J. Am. Chem. Soc.* **125**, 14298-14299 (2003).
19. C. G. Pappas *et al.*, *Nat. Nanotechnol.* **11**, 960-967 (2016).
20. J. Boekhoven, W. E. Hendriksen, G. J. Koper, R. Eelkema, J. H. van Esch, *Science* **349**, 1075-1079 (2015).
21. H. Zhao *et al.*, *Nat. Nanotechnol.* **11**, 82-88 (2016).

22. A. R. Hirst *et al.*, *Nat. Chem.* **2**, 1089-1094 (2010).
23. F. Trausel *et al.*, *Acc. Chem. Res.* **49**, 1440-1447 (2016).
24. Wang *et al.*, *Soft Matter* **7**, 10443–10448 (2011).
25. O. S. Lee, S. I. Stupp, G. C. Schatz, *J. Am. Chem. Soc.* **133**, 3677-3683 (2011).
26. G. Bellesia, J. E. Shea, *J. Chem. Phys.* **126**, 245104 (2007).
27. B. P. Partlow, M. Bagheri, J. L. Harden, D. L. Kaplan, *Biomacromolecules* (2016).
28. We used the solid phase sheets for DFY_{ox}, dispersed solution phase for spherical DYF_{ox} and the solution phases for FYD_{ox} and YFD_{ox} due to the presence of substantial starting materials in the solid phase for these materials [Fig. S16, Table S2].
29. H.-A. Park, Y. J. Kim, I. S. Kwon, L. Klosterman, C. J. Bettinger, *Polym. Int.* **65**, 1331-1338 (2016).
30. Y.J. Kim *et al.*, *Adv Mater.* **28**, :3173–3180 (2016).
31. G. M. Sheldrick, SHELXT–Integrated space-group and crystal-structure determination. *Acta Crystallogr. Sect. A* **71**, 3-8 (2015).
32. G. M. Sheldrick, A short history of SHELX. *Acta Crystallogr. Sect. A* **64**,112-122 (2008).

Acknowledgments

The research leading to these results has received funding from the US Air Force (AFOSR, grant FA9550-15-1-0192). A.L. is funded by the PBC, the Israeli Council for Higher Education. P.W.J.M is funded by Netherlands Organization for Scientific Research (Veni, 722.015.005). The authors are grateful for the support from the Materials Research Science and Engineering Center (MRSEC) program of the National Science Foundation (NSF) under Award Numbers DMR-0820341 and DMR-1420073 and for the assistance of Chun-Hsing (Josh) Chen in the University of Indiana, and Yu-Sheng Chen at the ChemMatCARS Sector 15 of the Advanced Photon Source (APS), which is principally supported by the NSF (grant number CHE-1346572). Use of the APS, an Office of Science User Facility operated for the U.S. Department of Energy (DOE) Office of Science by Argonne National Laboratory, was supported by the U.S. DOE under Contract No. DE-AC02-06CH11357. We thank A. Bykov (Department of Physics, City College of New York) for the help with WAXS analysis and J. Gu and V. M. Menon (Department of Physics, City College of New York) for the help with UV-Vis analysis. Hunter Mass Spectrometry is supported by the City University of New York, NSF, and the National Institute on Minority Health and Health Disparities (NIMHD) of the NIH. Results were obtained using the EPSRC funded ARCHIE-WeSt High Performance Computer (www.archie-west.ac.uk). EPSRC grant no. EP/K000586/1. The City University of New York has filed a provisional patent application (serial number 62/385,544) on technology related to this work.

Fig. 1. Sequence-dependent polymeric peptide pigments. (A) Schematic representation of the selected tripeptide sequences, and the controlled formation of polymeric peptide pigments by enzymatic oxidation and further polymerization of pre-organized tripeptides. (B) Macroscopic images of the materials formed by the self-assembly of the tripeptides (20 mM in phosphate buffer at pH 8) (upper panel), following 24 h (lower panel) of enzymatic oxidation (0.2 $\mu\text{g}/\mu\text{l}$), including oxidation of tyrosine as a control.

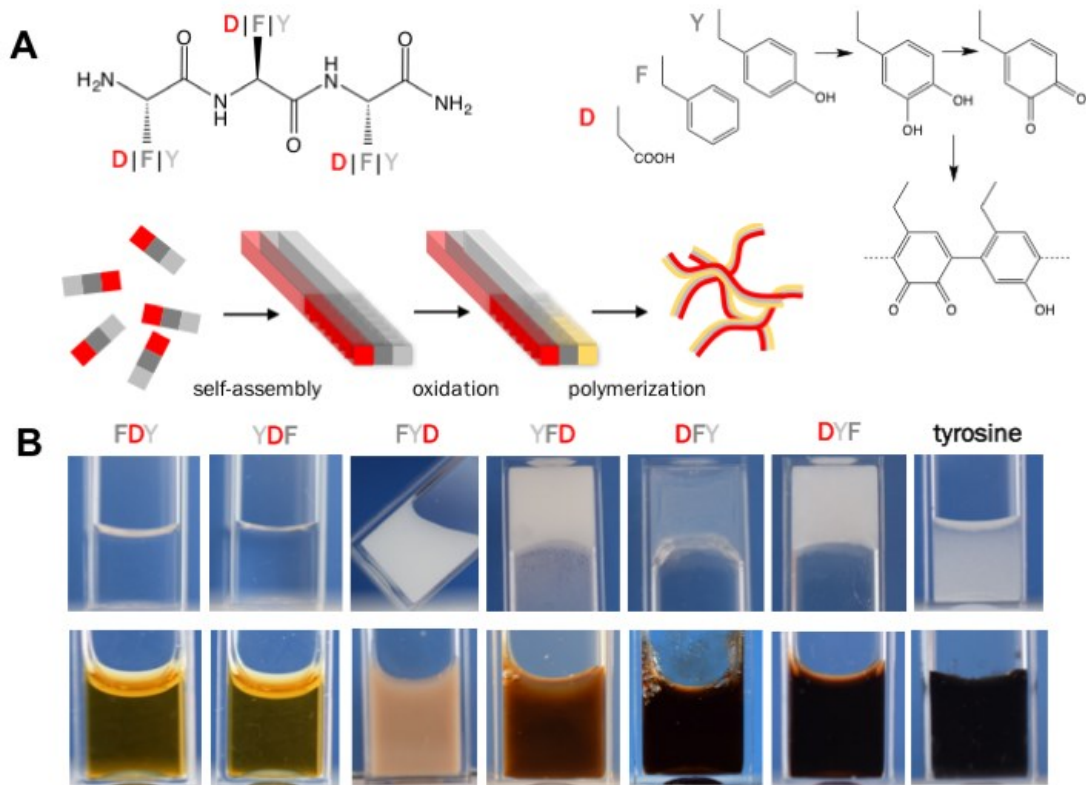


Fig. 2. Differential organization in tripeptide assemblies. (A) TEM micrographs of structures formed by self-assembly of tripeptides. Scale bars are 100 nm. (B-C) DYF (B) and YFD (C) crystal structure showing different interfaces forming the lattice (1-4 and main inset). (D) FTIR absorption spectra of the tripeptides (20 mM in D₂O phosphate buffer at pH 8). (E) Distribution of the CZ(Tyr)-CA(Tyr)-CA(Phe)-CZ(Phe) dihedral angle for each peptide over the course of 50 ns indicating the greatest populated angle. (F) Preferred conformations formed for each peptide.

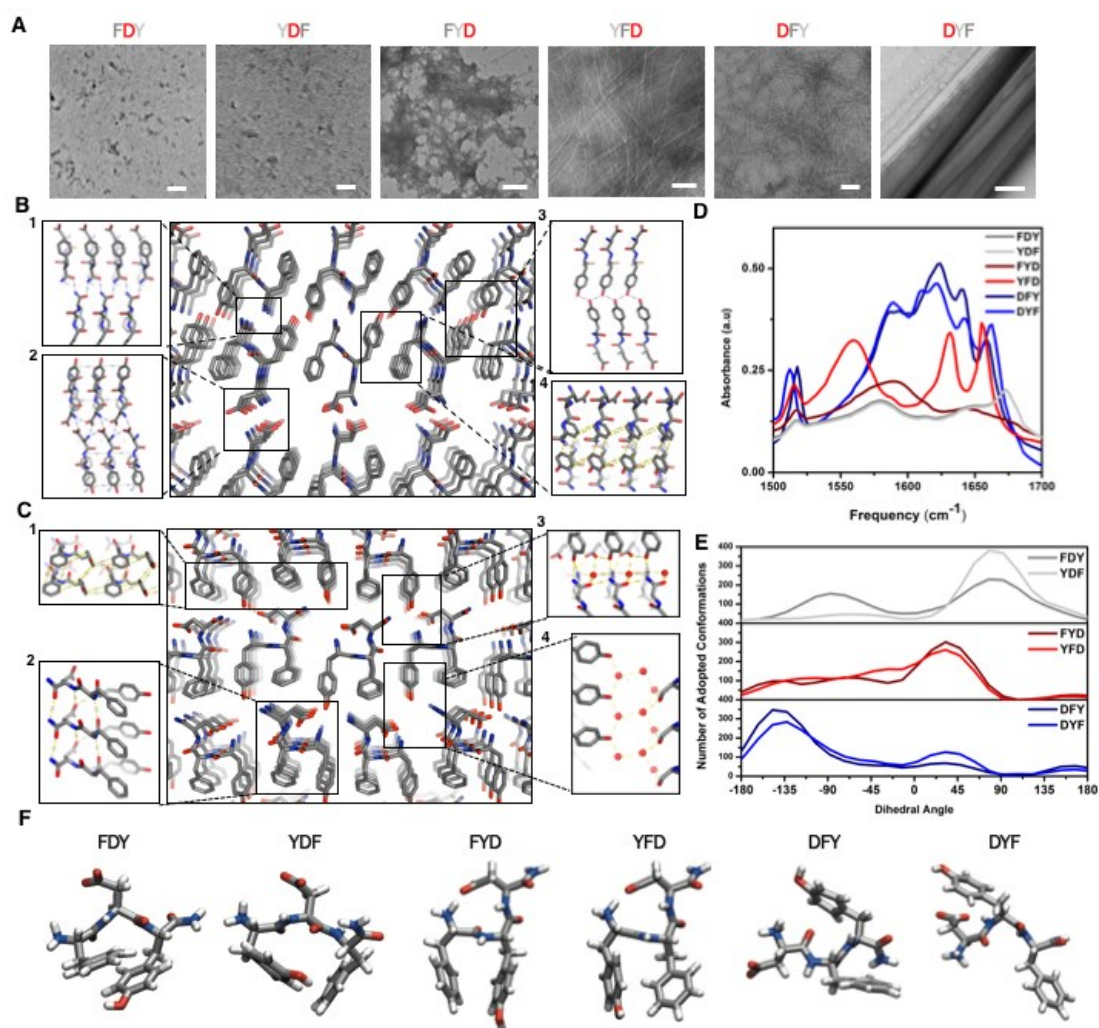


Fig. 3. From order to disorder in polymeric peptide pigments. (A-B) WAXS analysis including 1D (A) and 2D (B) patterns of tripeptides before (black) or after (red) 24 h of enzymatic oxidation. (C) FTIR absorption spectra of tripeptides before (solid lines) or after (dashed lines) 24 h of enzymatic oxidation. (D) LC-MS chromatograms 280 nm (black) 350 nm (red) of soluble fraction 24 h oxidized tripeptides. (E) Summed m/z intensities of soluble higher molecular weight polymers composed of heterogeneously connected monomers (F4) elute between 8-10 minutes. (F) Chemical structures of the non-oxidized peptides (1) and the oxidation products 3,4-dihydroxyphenylalanine (2) and 3,4-quinone (3) in the context of tripeptides. (4) Connectivity of potential aryl cross-linked and Michael addition products (see SI).

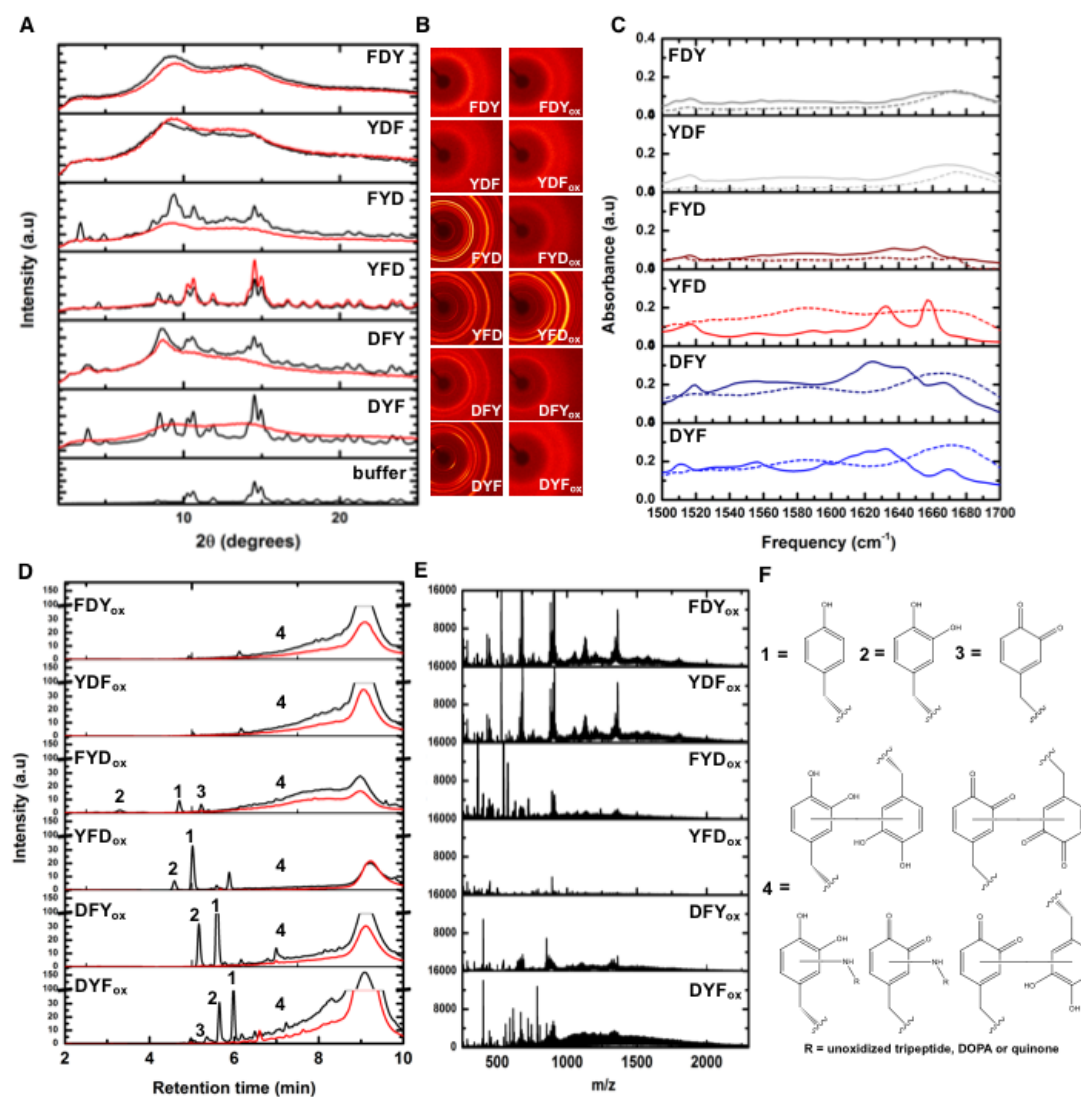


Fig. 4. Morphology, UV-Vis absorption and electrochemical properties of polymeric peptide pigments. (A) Structures formed by the polymeric peptide pigments at the micron scale using optical microscopy. Scale bars for FYD_{ox}, YFD_{ox} and DFY_{ox} are 20 μm and 10 μm for DYF_{ox}. (B) UV-Vis absorption spectra of solution fractions of polymeric peptide pigments or oxidized tyrosine. (C) Macroscopic image of polymeric peptide pigment electrode and schematic illustration of the electrochemical cell used for discharge measurements. (D) Electrochemical potential profiles and (E) average specific capacity of polymeric peptide pigments or oxidized tyrosine. Standard errors indicated, N=3.

